

3C-SiC(001)-3×2 Reconstructed Surface Analyzed by High-resolution Medium Energy Ion Scattering

T. Matsuda, M. Tagami, K. Mitsuhashi, A. Visikovskiy*, M. Shibuya and Y. Kido

Department of Physics, Ritsumeikan University, Kusatsu, Shiga-ken 525-8577, Japan

Abstract

The atomic structure of the 3C-SiC(001)-3×2 reconstructed surface was analyzed precisely by high-resolution medium energy ion scattering (MEIS). The present MEIS analysis unambiguously shows that the (3×2) surface consists of Si adatoms (1/3 ML, 1 ML = 1.05×10^{15} atoms/cm²) on top and underlying Si adlayer (2/3 ML) on the bulk truncated Si plane. As the result, the most probable structure is focused on the Two Adlayer Asymmetric Dimer Model predicted by *ab initio* calculations and the modified versions with alternating long and short dimers in the 2nd adlayer proposed by photoelectron diffraction (PED) and by grazing incidence X-ray diffraction (GIXRD) analyses. Observed MEIS spectra are well reproduced by the structure relatively close to that determined by PED rather than GIXRD. Interestingly, the first principles calculations using VASP (Vienna *ab initio* simulation package) prefers symmetric dimers in the second Si adlayer and non-relaxed interplanar distance between the top Si and 2nd C plane of the bulk-truncated surface, which are, however, unable to reproduce the observed MEIS spectra. The distorted 2nd adlayer (asymmetric dimers) may correlate with the compressed interplanar distance between the underlying Si and C plane.

* Present address: *Department of Applied Quantum Physics and Nuclear Engineering, Kyushu University, 744 Motoooka Nishi-ku, Fukuoka 819-0395, Japan*

I. INTRODUCTION

As well known, there are many polytypes of SiC with the same elemental composition and different stacking sequences, such as cubic, hexagonal 2H, 4H, 6H and so on. The electronic properties such as band gap and mobility are different significantly among them. As practical device applications, 4H-SiC substrates with a wide band gap and high mobility have been widely employed to fabricate Schottky diodes etc. Recently, however, the cubic SiC (3C-SiC) with the lowest band gap and fastest drift velocity has attracted much attention because of remarkable improvement of the crystalline quality realized by advanced chemical vapor deposition techniques. In addition, the growth on Si substrates has a great advantage to allow for device fabrication with a low cost.

Owing to dangling bonds of semiconductor surfaces, there exist many types of reconstructed surfaces for 3C-SiC(001)[1-5]. According to the report of Hara et al.[2], annealing 3C-SiC(001) at 700°C continuing Si deposition at a rate of 0.15 nm/min formed initially a (2×1) reconstructed surface and then led to a (3×2) reconstruction, which was kept down to room temperature (RT). By annealing the (3×2) surface at 1065°C for 4 min a (5×2) reconstruction appeared and additional annealing at 1065°C for 2 min resulted in a c(4×2) surface, which was gradually changed into the (2×1) structure at RT. Annealing at 1065°C in ultra-high vacuum (UHV) without Si deposition led to a c(2×2) surface. Auger electron spectroscopy coupled with medium energy ion scattering (MEIS) analysis confirmed that the (2×1), (3×2), (5×2) and c(4×2) surfaces were Si rich, while the c(2×2) surface was terminated with the C-plane[2].

There are many reports on the atomic structures of the above reconstructed surfaces analyzed mainly by electrons and X-ray diffraction techniques[1-3,6-10]. In this study, we analyze the relatively stable (3×2) reconstructed surface by high-resolution MEIS[11]. It is the advantage to use MEIS that the ion probe acts as entirely classical particles and thus simple geometrical consideration in a real space (trigonometry) needs only a few fitting parameters to best-fit the observed MEIS spectra[11,12], quite different from the diffraction methods. First we check all the structure models reported so far by high-resolution MEIS and then propose the most probable model, which is then compared with the *ab initio* calculations using VASP (Vienna *ab initio* simulation package)[13,14].

II. EXPERIMENT AND DATA ANALYSIS

As-supplied 3C-SiC(001) surfaces were first cleaned by modified RCA processing[15] and then degassed at 600°C for 5 hours by infrared radiation in UHV. Then annealed at 1050°C for 10 min to eliminate oxygen contaminations and after Si deposition of 6 ML (1 ML = 1.05×10^{15} atoms/cm²) further annealing at 950°C in UHV for 4 min led to clean (3×2) reconstructed surfaces, which were confirmed by reflection high-energy electron diffraction (RHEED). Here, the Si deposition was carried out with a Knudsen cell at a rate of ~0.5 ML/min. No significant O contaminations were checked by high-resolution MEIS.

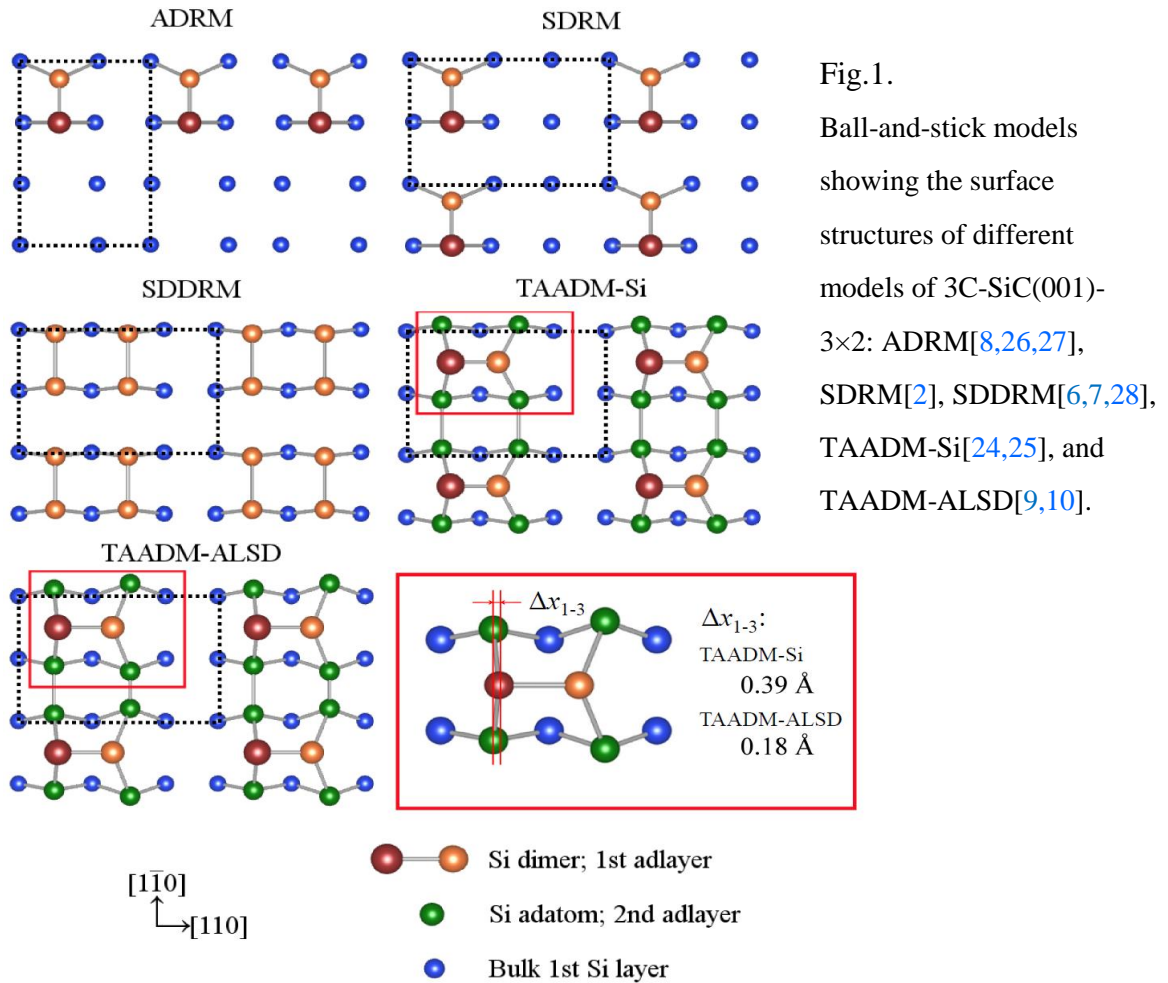
In the present MEIS analysis we employed a toroidal electrostatic analyzer (ESA) whose energy resolution $\Delta E/E$ was 1×10^{-3} (full width at a half maximum: FWHM)[11]. The corresponding depth resolution is estimated roughly to be ~0.01 nm, which depends on emerging angle of scattered ions. We employed 120 keV He⁺ ions which were collimated to 0.18 and 2.0 mm, respectively in the horizontal and vertical plane. The sample was biased at +90 V to suppress secondary electron emission and the ion irradiated position on the sample surface was shifted after an integrated beam current of 1 μ C to minimize radiation damage and sputter etching effects. The effects of this applied voltage upon scattered He⁺ energy and emerging angle were negligibly small, roughly estimated to be less than 10 eV and 0.1°, respectively. The sample preparation and ion scattering chambers were kept in UHV condition ($\leq 2 \times 10^{-10}$ Torr).

The yield of He⁺ ions scattered from target atoms j with an energy E is expressed by

$$Y_j(E) = Q (d\sigma/d\Omega)_j \rho_j \Delta x \Delta\Omega \varepsilon \eta_+ P_{CL}^{(j)} / \cos \theta_{in}, \quad (1)$$

where Q , $(d\sigma/d\Omega)_j$, $\Delta\Omega$, ε , and θ_{in} , respectively are number of incident He⁺ ions, scattering cross section, solid angle subtended by the toroidal ESA (7.64×10^{-5} str), detection efficiency (0.44) and incident angle with respect to surface normal. Here, η_+ is the He⁺ fraction for scattered He ions (He⁰, He⁺, He²⁺) dependent on emerging energy and angle, which was measured in advance[16]. The areal density (atoms/cm²) of target atoms j of interest is expressed by $\rho_j \Delta x$ and $P_{CL}^{(j)}$ corresponds to the close encounter (hitting) probability for the atoms j . The close encounter probability for the atoms in each layer was normalized by that for the atoms which were not shadowed (e.g. atoms on top of the surface) and that was calculated from Monte Carlo (MC) simulations of

ions trajectories assuming the subsurface ordered structure including the (3×2) reconstructed layers. In the MC simulations, we considered thermal vibrations (TV) whose root mean square TV amplitudes for C and Si were calculated from the Debye temperature of 1200 K for 3C-SiC[17] and used the inter-atomic potentials given by Ziegler-Biersack-Littmark called ZBL potentials for short[18]. A MEIS spectrum is easily constructed, if the subsurface structure is given explicitly[19,20]. We employed the asymmetric line shapes expressed by an exponentially modified Gaussian profile (EMG)[21,22] and energy straggling formula given by Lindhard-Scharff[23]. The stopping powers are approximated by Ziegler's stopping powers $S_Z(E)$ [18] multiplied by 1.30 and 0.79 for C and Si, respectively, which were measured in advance using amorphous-C(~ 100 Å)/Si(111) and amorphous-Si(~ 20 Å)/graphite. Rutherford backscattering with 1.5 MeV He^+ ions determined the thicknesses of the a-C and a-Si films.



The best-fit to an observed MEIS spectrum is evaluated quantitatively by the R -factor defined by

$$R \equiv \frac{\sum_i \left\{ \left| Y_j^{EXP}(E_i) - Y_j^{SIM}(E_i) \right| \cdot (Y_j^{EXP}(E_i) / Y_j^{Max}) \right\}}{\sum_i Y_j^{(EXP)}(E_i)}, \quad (2)$$

where $Y_j^{EXP}(E_i)$ and $Y_j^{SIM}(E_i)$, respectively are observed and simulated yields for He^+ ions scattered from atoms j with an energy E_i and Y_j^{Max} is the observed maximum yield for He^+ ions scattered from atoms j in the energy range of interest. In the present MEIS analysis our concern is focused on the energy spectra for He^+ ions scattered from Si atoms.

III. THE STRUCTURE MODELS FOR THE 3C-SiC(001)-3×2

There are many structure models proposed so far for the 3C-SiC(001)-3×2 reconstructed surface[2,6-10]. *Ab initio* calculations to optimize the (3×2) surface structure has been also performed by Pollmann and coworkers[24,25] and others[26,27]. Now we show the representative structure models by ball and stick models in Fig. 1; (i) Alternate Dimer Row Model (ADRM)[8,26,27], (ii) Single Dimer Row Model (SDRM)[2], (iii) Symmetric Double Dimer Row Model (SDDRM)[6,7,28], (iv) Two Adlayer Asymmetric Dimer Model-for Si-terminated surfaces (TAADM-Si)[24,25] and (v) Two Adlayer Asymmetric Dimer Model-Alternating Long and Short Dimer (TAADM-ALSD)[9,10]. The ADRM and SDRM surfaces have one single dimer in the (3×2) unit cell with a Si coverage of 1/3 ML. In the ADRM, the dimers in the adlayer are arranged in an alternate way to form a (2×3) reconstruction and thus the dimer direction is parallel to the ×3 ($[\bar{1}10]$) direction. The SDDRM surface involves two symmetric dimers (2/3 ML) in the unit cell on a bulk truncated Si layer. The TAADM structure is basically the ADRM (3×2) reconstructed layer built on top of the SDDRM and thus the reconstructed surface comprises 1 ML Si (1/3 + 2/3 ML).

Historically, Dayan first observed the (3×2) reconstructed surface by low and high energy electron diffraction (LEED & RHEED) combined with Auger electron spectroscopy and proposed the SDDRM structure[6]. Hara et al.[2] first suggested the SDRM reconstruction based on LEED combined with MEIS. However, they could not explain the images of scanning tunneling microscopes (STM)[7,8] and thus supported the SDDRM reconstruction. On the other hand, the *ab initio* calculations[26,27]

predicted the ADRM structure more energetically stable than SDRM, which was also supported by the STM observation[8]. Here, we must note that STM cannot give three dimensional structure information, besides the lateral atomic distribution. Recently, however, Lu et al.[24] proposed the TAADM-Si structure with a coverage of 1 ML Si which is the most stable (3×2) reconstruction among the above configurations. Then D'Angelo et al.[9] checked the validity of the TAADM-Si structure by grazing incidence X-ray diffraction (GIXRD) and found the modified version of the TAADM-Si as the most probable structure, which involves alternating long and short dimers in the second plane (TAADM-ALSD). This reconstruction was confirmed by soft X-ray photoelectron diffraction (PED)[10].

IV. RESULTS AND DISCUSSION

A. *Ab initio* calculations

The *ab initio* calculations based on the density functional theory (DFT) have been carried out using VASP, in which the generalized gradient approximation (GGA)[29] as the exchange-correlation potentials and projector-augmented wave (PAW) method[30] as the basis functions were employed. We adopted the Residual Minimization/Direct Inversion in the Iterative Subspace (RMM-DIIS) algorithm[31] as an efficient electronic minimization and applied conjugate gradient method[32] to optimize rapidly the configuration of ion cores. The cut-off energy for the plane-wave basis was set to 500 eV. For \vec{k} point sampling to perform fast Fourier transform, 5×7×1 Monkhorst-Pack mesh[33] was used. The calculations were terminated when the Hellmann-Feynman force acting on each atom is less than 0.05 eV/Å. We checked the validity of the above choice by comparing the calculated bulk bond length with the experimental value.

As the initial condition, three atomic configurations were assumed which consisted of the two adlayer asymmetric dimer structures corresponding to TAADM-Si[24], -ALSD-GIXRD[9] and -ALSD-PED[10] and thus the 3C-SiC(001)-3×2 super cell comprised two Si adlayers, four Si-C bilayers and a Si-H bilayer to terminate the dangling bonds of the backside surface, because as shown later, the present MEIS analysis reveals the presence of Si adatoms (1/3 ML) on top and underlying Si adlayer (2/3 ML) on the bulk truncated Si plane. The vacuum spacing of 10 Å was inserted between neighboring unit cells to avoid interactions between the unit cell slabs. The lateral size of the unit cell was determined by the calculated result for the 3C-SiC bulk

(lattice constant $a = 4.36 \text{ \AA}$ [34]). The optimized structures for the above three initial conditions converged into almost the same atomic configuration, which is shown in Table 1. The structure given by the present VASP calculation coincides well with that predicted by Lu et al.[24] (TAADM-Si).

B. MEIS analysis

Figure 2 shows the observed MEIS spectrum for 120keV He^+ ion incident at 54.7° and scattered to 86.0° scaled from the surface normal and scattered from Si atoms. The thick solid and dotted curves correspond to the simulated spectra assuming the SDDRM[7] and TAADM-ALSD-PED[10]. The incident direction (54.7°) along the $[1\bar{1}1]$ -axis was chosen to suppress the scattering components from Si atoms in the deeper layers and to make clear the surface peaks mainly from the Si atoms in the (3×2) reconstructed surface. In addition the grazing emergence geometry improves a depth resolution and makes it possible to separate the scattering components from Si in each atomic layer. The surface peak is decomposed into the scattering components (thin solid curves) from the long and short dimers in the first adlayer (1/3 ML), the second adlayer (2/3 ML) and from the top (1 ML), second (1 ML) and deeper layers of the bulk truncated SiC(001) surface. As can be seen from the figure, the SDDRM surface (dotted curve) consisting of 2/3 ML Si adlayer cannot reproduce well the observed surface peak from Si (open circles) and presence of additional 1/3 ML of Si leads to a good fit to the observed surface peak. Therefore, the ADRM and SDRM surfaces with fewer amounts of Si adatoms are ruled out.

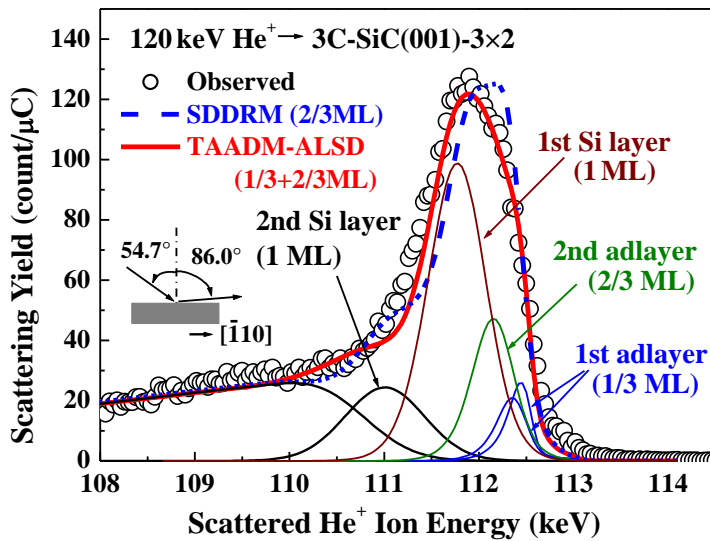


Fig. 2. MEIS spectrum observed for 120 keV He^+ ions incident on the 3C-SiC(001)- 3×2 surface at an angle of 54.7° and scattered to 86° in the (110) plane (open circles). Simulated spectra assuming SDDRM and TAADM-ALSD are indicated by dotted and solid curves, respectively. Thin curves correspond to scattering components from each atomic layer of TAADM-ALSD surface.

Figures 3(a) and (b), respectively indicate the observed MEIS spectra for 120 keV He^+ ion incident along the $[1\bar{1}1]$ -axis and scattered to 85° and incident along the $[0\bar{1}1]$ -axis and scattered to 86° . The Solid and dotted curves are the simulated MEIS spectra assuming the TAADM-ALSD-PED[10] and the TAADM-Si[24], respectively. As illustrated in Figs. 1 and shown in Table 1, the pronounced difference between the TAADM-Si and TAADM-ALSD-PED resides in the dimer length in the second adlayer and the lateral shift of the upper Si atom of the top dimer in the $[110]$ direction from the 2nd layer Si row along $[1\bar{1}0]$ -axis denoted by Δx_{l-3} . The symmetric dimers in the TAADM-Si generate the larger scattering yield from the Si atoms in the 2nd adlayer than that for the TAADM-ALSD-PED. Indeed, the MC simulations of ion trajectories showed that the He^+ ions scattered from the Si atoms in the 2nd-adlayer (numbered 3 in Fig. 4) undergo a strong focusing effect ($P_{CL} = 1.56$) by overlying Si dimers (numbered l' in Fig. 4) for the TAADM-Si surface, whereas they receive a significant blocking effect ($P_{CL} = 0.80$) for the TAADM-ALSD-PED. The blocking and focusing effects are much sensitive to Δx_{l-3} and thus change the height of the surface peak. It is clearly seen that the TAADM-ALSD-PED reproduces well the observed MEIS spectrum shown in Fig. 3(a), while the TAADM-Si gives the higher surface peak than the observed one. In the case of the $[01\bar{1}]$ incidence (Fig. 3(b)), the TAADM-ALSD-PED does not give the best-fit of the surface peak to the observed one, although reproduces well the shoulder part. Another version of the TAADM-ALSD-GIXRD[9] also does not give a good fit to the observed MEIS spectra. Obviously the TAADM-Si cannot simulate well the observed surface peak as well as the shoulder. The *ab initio* calculations performed at 0 K tend to give a lower total energy by taking a higher symmetric structure for the 2nd adlayer. This does not match sometimes the surface structure observed at room temperature. The situation is different from that for the top Si layer. The Si atoms with dangling bonds in the 1st adlayer take the asymmetric dimer structure as the ground state, just like the Si(001)- 2×1 surface even at temperatures close to 0 K[35,36].

The above MEIS spectrum analysis suggests that the observed spectra can be fitted well by a modified version of the TAADM-ALSD structures. As mentioned before, the scattering geometry taken for Fig. 3(a) is sensitive to the lateral shift (Δx_{l-3}) of the upper Si atoms of the top dimers (see Fig. 1), while not very sensitive to the interlayer distance between the top and 2nd adlayer (Δ_{l-II}). Indeed, in the scattering in the (110) plane (Fig. 3(a)) at emerging angle of 85° , the He^+ ions scattered from the Si atoms

numbered 3 are slightly blocked by the upper Si atoms of the top dimers numbered I' (see Fig. 4) for the TAADM-ALSD-PED, while they undergo a strong focusing effect for the TAADM-Si. The scattering in the (010) plane ([100]-azimuth) at emerging angle of 86° (see Fig. 4) is sensitive to the bond length of the shorter dimer (d_{5-6}) in the 2nd adlayer and also to the interlayer distance (Δ_{II-III}) between the 2nd Si adlayer and the top Si layer of the bulk truncated SiC(001) surface. Actually the height of the primary surface peak is dependent on the geometry of the Si atoms numbered II in the 1st Si layer relative to the Si atoms of the shorter dimer numbered 5 in the 2nd adlayer (see Fig. 4). The He^+ ions scattered from the Si atoms numbered II are significantly blocked by the Si atoms numbered 5 ($P_{CL} = 0.87$) for the TAADM-ALSD-PED surface, while subjected to a slight focusing effect ($P_{CL} = 1.16$) for the TAADM-Si. If the 2nd layer Si atoms are not shadowed by the overlying Si atoms in the 2nd adlayer, the shoulder on the lower energy side in Fig. 3(b) appears. This scattering geometry is sensitive to Δ_{II-III} and the interlayer distance (Δ_{III-IV}) between the top Si and C planes of the bulk truncated SiC(001) surface.

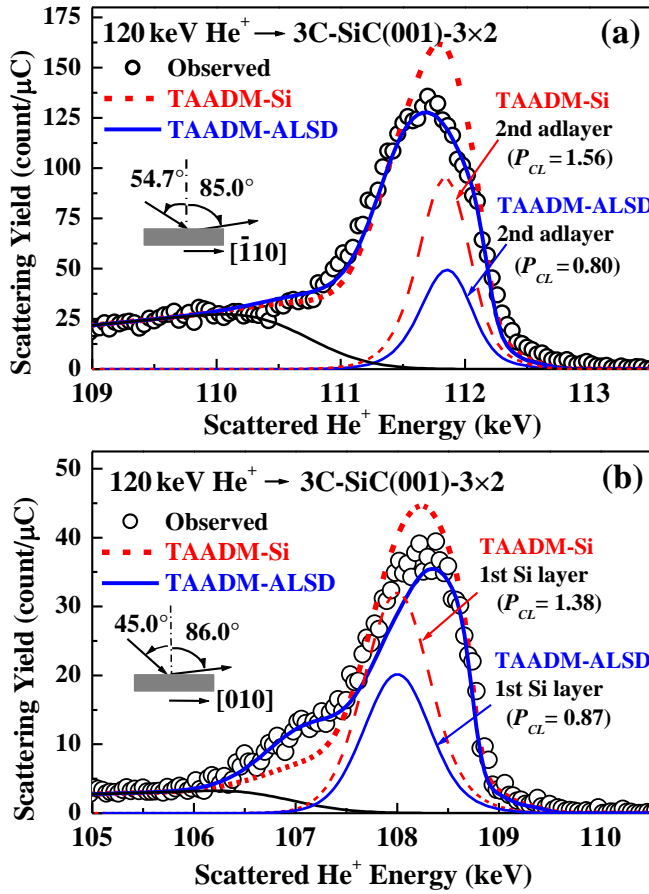


Fig.3. MEIS spectrum observed for 120 keV He^+ ions incident (a) at angle of 54.7° and scattered to 85° in the (110) plane and (b) at angle of 45.0° and scattered to 86° in the (010) plane. Thick solid and dotted curves, respectively are simulated spectra assuming TAADM-Si and -ALSD. Thin solid curves denote scattering components from 2nd Si adlayer and Si atoms below 2nd Si layers of bulk truncated SiC(001) surface.

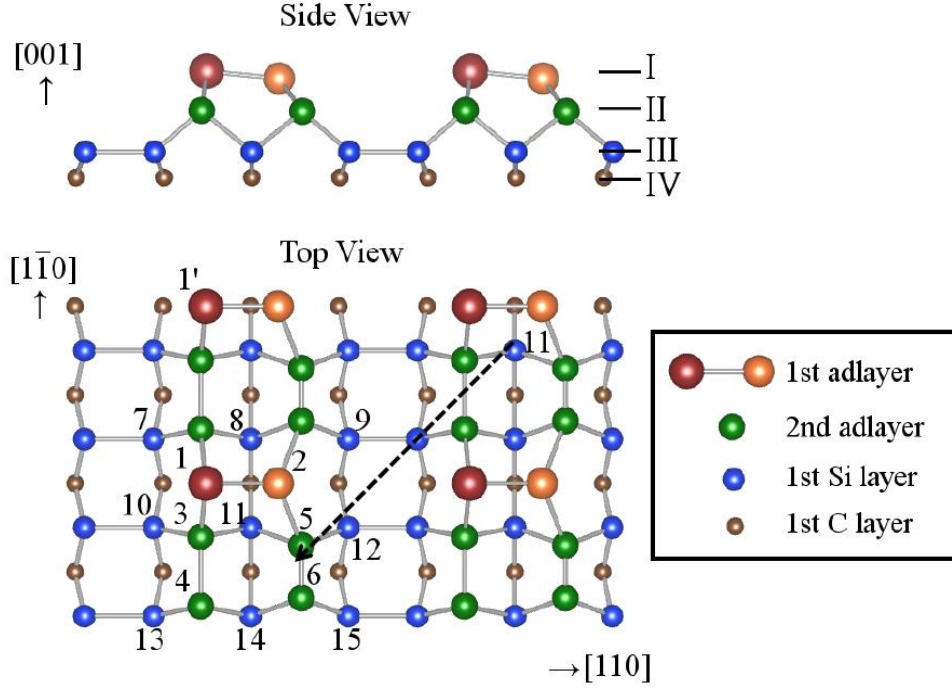


Fig. 4. Top and side views of TAADM-ALSD reconstructed surface.

We first assume the TAADM-ALSD-PED[10] surface except for the bond length of the shorter dimer (d_{5-6}) and average interlayer distance between the 2nd adlayer and 1st Si layer (Δ_{II-III}) and simulated the MEIS spectra varying d_{5-6} and Δ_{II-III} . The R -factors are calculated for three MEIS spectra observed at incident angle of 54.7° and scattered to 86° (Fig. 2) and 85° (Fig. 3(a)) and at incident angle of 45° and scattered to 86° (Fig. 3(b)) by setting the energy range of interest from 110.0 to 113.5 keV, from 109.0 to 113.0 keV and from 106.0 to 110.0 keV, respectively. The total R -factors evaluated for three MEIS spectra are indicated in Fig. 5(a). Obviously, the values of $\Delta_{II-III} = 1.50 \pm 0.02$ Å and $d_{5-6} = 2.00 \pm 0.05$ Å minimize the R -factor and significantly differ from those determined by photoelectron diffraction[10]. Concerning the lateral shift Δx_{1-3} , the best choice was 0.18 - 0.20 Å. Here, we must note that the present MEIS analysis is not very sensitive to d_{1-2} , Δz_{1-2} and Δ_{I-II} and there is no significant difference in the bond length of the longer dimer (d_{3-4}) for the TAADM and *ab initio* calculations (see Table 1). There is also difference in Δ_{III-IV} (inter-planar distance between top Si and 2nd C plane of bulk truncated SiC(001)) for the TAADM-ALSD and *ab initio* calculations (see Table 1). So, we fixed the optimum

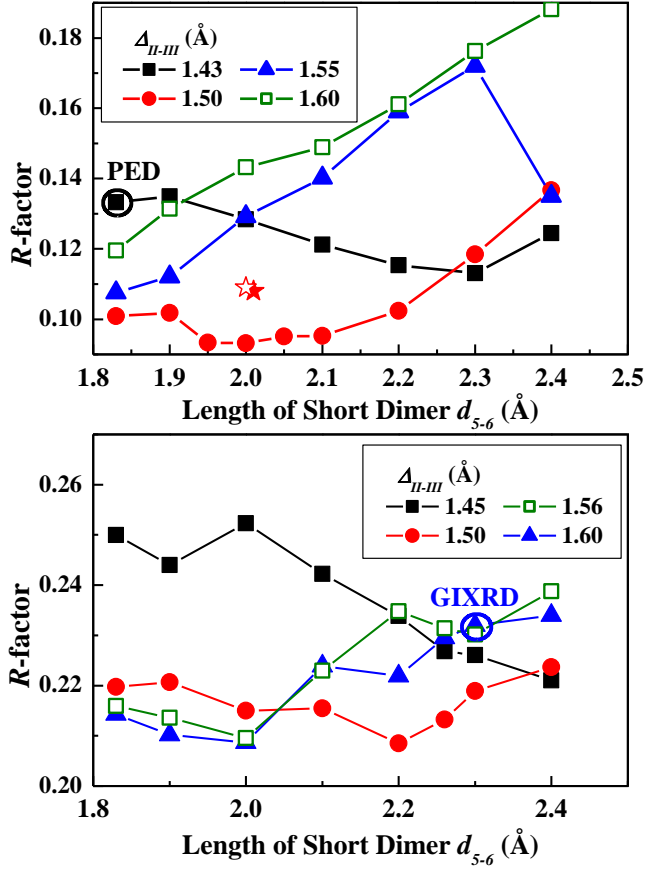


Fig. 5. (a) R -factors calculated assuming basically the atomic configuration given by TAADM-ALSD-PED[10] and varying bond length of short Si dimer (abscissa) and interlayer distance (Δ_{II-III}) between 2nd adlayer and 1st Si layer of bulk truncated SiC(001) surface. Open and filled asterisks denote the R -factors obtained for $\Delta_{III-IV} = 1.0$ and 0.80 Å, respectively. (b) R -factors calculated assuming basically the atomic configuration given by TAADM-ALSD-GIXRD[10] and varying bond length of short Si dimer (abscissa) and Δ_{II-III} .

values of $d_{5-6} = 2.00$ and $\Delta_{II-III} = 1.50$ Å and varied Δ_{III-IV} from 0.8 to 1.0 Å. Interestingly, the R -factor is minimized at $\Delta_{III-IV} \cong 0.9$ Å more than 20 % shorter than the bulk interplanar distance of 1.09 Å. The best-fit condition is indicated as MEIS(I) in Table I. In contrast, the present VASP calculations give the Δ_{III-IV} value of 1.09 Å coinciding with the 3C-SiC bulk interplanar distance, which is consistent with the prediction (1.06 Å) by Lu et al.[24]. The distorted (asymmetric) structure in the 2nd adlayer may correlate with the compressed interplanar distance between the underlying Si and C plane. Next we evaluated the R -factors assuming the atomic configuration determined by TAADM-ALSD-GIXRD[9] except for the values of d_{5-6} and Δ_{II-III} and the results are indicated in Fig. 5(b). The R -factor is minimized at a smaller length (~ 2.0 Å) of the shorter dimer than that (2.26 Å) determined by GIXRD and the minimized R -factor is considerably larger than that obtained based on the TAADM-ALSD-PED, as indicated in Fig. 5(a). This degraded R -factor values are attributed to the Δx_{1-3} value (0.54 Å) considerably larger than those adopted in MEIS(I) and also to different Δ_{II-III} and Δ_{III-IV} values (see Table I). However, simply making these three values close to those of MEIS(I) in Table I did not reduce the

R -factor effectively. As discussed above, the most probable atomic configuration determined by the high-resolution MEIS is basically closer to the TAADM-ALSD-PED structure rather than the TAADM-ALSD-GIXRD and TAADM-Si, although significantly different in the d_{5-6} and Δ_{II-III} values. The best-fitted MEIS spectra are obtained assuming $d_{5-6} = 2.00$, $\Delta_{II-III} = 1.50$, $\Delta_{III-IV} = 0.89$ and $\Delta x_{1-3} = 0.2$ Å, as shown in Figs. 6(a), (b) and (c) (see also Table I).

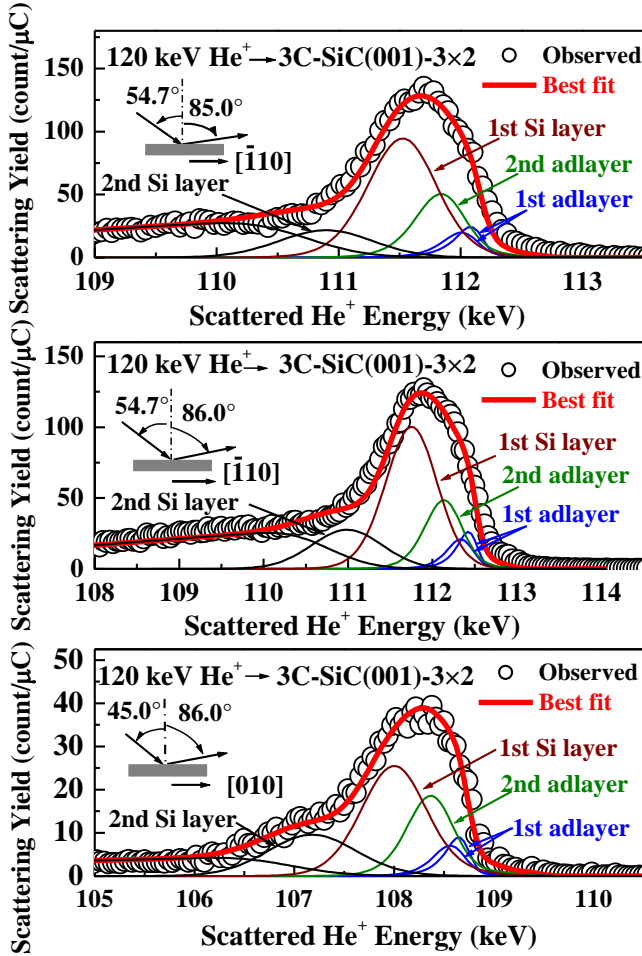


Fig.6.

MEIS spectrum observed for 120 keV He^+ ions incident (a) at angle of 54.7° and scattered to 85° in (110) plane and (b) at angle of 54.7° and scattered to 86° in (110) plane and (c) at angle of 45.0° and scattered to 86° in the (010) plane. Thick curves correspond to best-fitted spectra (total) assuming the most probable atomic configuration given in Table 1. Thin solid curves denote scattering components from each layer of reconstructed and bulk truncated SiC(001) surface.

V. CONCLUSION

The present MEIS analysis using the shadowing and blocking effects demonstrates that the 3C-SiC(001)-3x2 reconstructed surface takes the atomic configuration consisting of asymmetric dimer in the 1st Si adlayer (1/3 ML) and alternating long and short dimer in the 2nd Si adlayer (2/3 ML) namely the TAADM-ALSD structures. The most probable structure reproducing well the observed MEIS spectra is relatively close to the TAADM-ALSD structure determined by PED rather than that given by GIXRD.

However, the length of the short dimer (d_{5-6}) and the interlayer distance (Δ_{II-III}) between the 2nd adlayer and the top Si plane of the bulk truncated SiC(001) surface respectively are 10 and 5 % larger than those of TAADM-ALSD-PED. Interestingly, the present MEIS as well as the PED analysis give much shorter interplanar distance (Δ_{III-IV}) more than 20 % between the top Si and 2nd C plane of the bulk-truncated SiC(001) surface than that predicted by DFT calculations, which coincides with the bulk interplanar distance. Another interesting issue is the fact that the *ab initio* calculations prefer a higher symmetric structure for the 2nd adlayer, which, however, cannot reproduce the observed experimental data. The distorted (asymmetric) structure probably correlates with the compressed interplanar distance between the underlying Si and C plane.

Table 1. Parameters defining the SiC(001)-3×2 reconstructed surface, d_{i-j} is the dimer length between the Si atoms numbered i and j in Fig. 4, Δz_{I-2} is the height difference of the asymmetric top dimer, Δ_{I-J} is the interlayer distance between the I -th and J -th layer and Δx_{I-3} is the lateral shift of the upper Si atom of the top dimer in the [110] direction from the 2nd layer Si row along $[1\bar{1}0]$ -axis (see Fig. 1). The values in parentheses are assumed ones in the MEIS analysis.

Parameters (Å)	MEIS(I)	MEIS(II)	DFT (Present)	DFT [23]	GIXRD [9]	PED [10]
d_{I-2}	(2.78)	(2.54)	2.33	2.24	2.78±0.03	2.54±0.10
Δz_{I-2}	(0.10)	(0.25)	0.65	0.50	0.10±0.05	0.25±0.10
d_{3-4}	(2.41)	(2.40)	2.49	2.38	2.41±0.08	2.40±0.10
d_{5-6}	2.00±0.05	2.00±0.05	2.45	2.37	2.26±0.08	1.83±0.20
Δ_{I-II}	(1.56)	(1.26)	1.27	1.19	1.56±0.04	1.26±0.05
Δ_{II-III}	1.58±0.02	1.50±0.02	1.62	1.59	1.56±0.04	1.43±0.05
Δ_{III-IV}	(1.09)	0.89±0.02	1.09	1.06		0.89±0.05
Δx_{I-3}	(0.54)	0.18 - 0.20	0.34	0.39	0.54	0.18

Acknowledgements

The authors would like to appreciate M. Kohyama for his valuable comments on the first principles calculations. Thanks are also due to H. Okumura for his assistant in the MEIS experiment. This work was partly supported by the Ministry of Education, Japan, ‘Academic Frontier Project’.

References

- [1] R. Kaplan, Surf. Sci. **215** (1989) 111.
- [2] S. Hara, W.F.J. Slijkerman, J.F. van der Veen, I. Ohdomari, S. Misawa, E. Sakuma and S. Yoshida, Surf. Sci. Lett. **231** (1990) L 196.
- [3] J.M. Powers, A. Wander, P.J. Rous, M.A. van Hove and G.A. Somorjai, Phys. Rev. **B 44** (1991) 11159.
- [4] P. Soukiassian, Mat. Sci. Eng. **B 61-62** (1999) 506.
- [5] A. Catellani and G. Galli, Prog. Surf. Sci. **69** (2002) 101.
- [6] M. Dayan, J. Vac. Sci. Technol. **A 4** (1986) 38.
- [7] S. Hara, S. Misawa, S. Yoshida and Y. Aoyagi, Phys. Rev. **B 50** (1994) 4548.
- [8] F. Semond, P. Soukiassian, A. Mayne, G. Dujardin, L. Douillard and C. Jaussaud, Phys. Rev. Lett. **77** (1996) 2013.
- [9] M. D'Angelo, H. Enriquez, V.Yu. Aristov, P. Soukiassian, G. Renaud, A. Barbier, M. Noblet, S. Chiang and F. Semond, Phys. Rev. **B 68** (2003) 165321.
- [10] A. Tejada, D. Dunham, F.J. Garcia de Abajo, J.D. Denlinger, E. Rotenberg, E.G. Michel and P. Soukiassian, Phys. Rev. **B 70** (2004) 045317.
- [11] Y. Kido, T. Nishimura, Y. Hoshino and H. Namba, Nucl. Instrum. Methods **B 161-163** (2000) 371.
- [12] J.F. van der Veen, Surf. Sci. Rep. **5** (1985) 201.
- [13] G. Kresse and J. Hafner, Phys. Rev. **B 47** (1993) 558.
- [14] G. Kresse and J. Furthmüller, Phys. Rev. **B 54** (1996) 11169.
- [15] W. Kern and D.A. Puotinen, RCA Rev. **31** (1970) 187.
- [16] Y. Kitsudo, K. Shibuya, T. Nishimura Y. Hoshino, I. Vickridge and Y. Kido, Nucl. Instrum. Methods **B 267** (2009) 56.
- [17] *Properties of Advanced Semiconductor Materials GaN, AlN, SiC, BN, SiC, SiGe*, Eds. M.E. Levinshtein, S.L. Rumyantsev, M.S. Shur (John Wiley & Sons, Inc., New York, 2001).
- [18] J.F. Ziegler, J.P. Biersack and W. Littmark, *The Stopping and Range of Ions in Matter* (Pergamon, New York, 1985).
- [19] Y. Kido and T. Koshikawa, J. Appl. Phys. **67** (1990) 187.
- [20] T. Nishimura, A. Ikeda, H. Namba and Y. Kido, Surf. Sci. **411** (1998) L834.
- [21] P.L. Grande, A. Hentz, R.P. Pezzi, I.J.R. Baumvol, G. Schiwietz, Nucl. Instrum. Methods **B 256** (2007) 92.

- [22] M. Hazama, Y. Kitsudo, T. Nishimura, Y. Hoshino, P.L. Grande, G. Schiwietz and Y. Kido, Phys. Rev. B **78** (2008) 193402.
- [23] J. Lindhard and M. Scharff, Kgl. Danske. Vidensk. Selsk. Mat.-Fys. Medd. **27** (15)(1953) 1.
- [24] W. Lu, P. Krüger and J. Pollmann, Phys. Rev. B **60** (1999) 2495.
- [25] P. Krüger and J. Pollmann, Phys. Rev. B **73** (2006) 035327.
- [26] H. Yan, A.P. Smith and H. Jónsson, Surf. Sci. **330** (1995) 265.
- [27] L. Pizzagalli, A. Catellani, G. Galli, F. Gygi and A. Baratoff, Phys. Rev. B **60** (1999) R5129.
- [28] H.W. Yeom, Y.C.-. Chao, S. Terada, S. Hara, S. Yoshida and R.I.G. Uhrberg, Phys. Rev. B **56** (1997) R15525.
- [29] J.P. Perdew, K. Burke and M. Ernzerhof, Phys. Rev. Lett. **77** (1996) 3865.
- [30] P.E. Blöchl, Phys. Rev. B **50** (1994) 17953.
- [31] G. Kresse and J. Furthmüller, Phys. Rev. B **54** (1996) 11169.
- [32] D.M. Bylander, L. Kleinman, and S. Lee, Phys. Rev. B **42** (1990) 1394.
- [33] H.J. Monkhorst and J.D. Pack, Phys. Rev. B **13** (1976) 5188.
- [34] *Silicon Carbide - A High Temperature Semiconductor*, eds. J.R. O'Connor and J. Smiltens, (Pergamon Press, New York, 1960).
- [35] A. Ramstadt, G. Brocks and P.J. Kelly, Phys. Rev. B **51** (1995) 14504.
- [36] K. Sagisaka, M. Kitahara, D. Fujita, G. Kido and N. Koguchi, Nanotechnology **15** (2004) S371.